

STUDY OF AN ALGORITHM BASED ON MODEL EXPERIMENTS AND DIFFUSION THEORY FOR A PORTABLE TISSUE OXIMETER

Toshikazu Shiga,[†] Katsuyuki Yamamoto,[‡] Kazuhisa Tanabe,[†] Yuzo Nakase,^{*} and Britton Chance^{**}

[†]Omron Institute of Life Science Co. Ltd., 24, Yamanouti Yamanoshita-cho, Ukyo-ku, Kyoto 615, Japan; [‡]Hokkaido University, Faculty of Engineering, Sapporo 060, Japan; ^{*}Omron Corporation, Tokyo 105, Japan; ^{**}University of Pennsylvania, Johnson Research Foundation, Philadelphia, Pennsylvania 19104

(Paper JBO/NIR-15 received July 8, 1996; revised manuscript received Jan. 2, 1997; accepted for publication Jan. 22, 1997.)

ABSTRACT

A portable tissue oximeter that uses light-emitting diodes and two-wavelength near infrared spectroscopy has been developed. The tissue oximeter is compact enough to be portable and it is therefore expected to make better use of the advantages of NIRS-based oximetry and to expand the scope of applications of monitoring tissue oxygen. The algorithm for this instrument was deduced through systematic experiments by varying blood volume and scattering intensity in a tissuelike phantom. The experimental results were compared with theoretical results obtained from diffusion theory. Experimentally determined coefficients of the algorithm were in close agreement with the theoretically derived coefficients. From evaluation tests of the algorithm applied to *in vitro* and *in vivo* measurements, it was confirmed that a good linear response to the concentration of oxygenated and deoxygenated blood can be obtained by this algorithm within a range of about a 50% change in concentration from an initial state. © 1997 Society of Photo-Optical Instrumentation Engineers. [S1083-3668(97)00102-0]

Keywords near infrared spectroscopy; oximeter; portable monitor.

1 INTRODUCTION

Tissue oximeters using near infrared spectroscopy (NIRS) can continuously determine the concentrations of oxygenated and deoxygenated hemoglobin in a noninvasive manner. Owing to these characteristics, this type of oximeter is now becoming widely used for clinical applications, primarily for monitoring cerebral oxygenation in adults^{1-3,8} and neonates.⁴⁻⁷ Tissue oximeters have also begun to be used for diagnosing impaired peripheral circulation associated with peripheral vascular disease (PVD)⁹ or heart failure,¹⁰ arteriosclerosis obliterans (ASO),¹¹ and mitochondrial myopathy,¹² and for assessing the recovery of skeletal muscle activity in patients undergoing rehabilitation.¹³ Owing to the noninvasiveness and simplicity of the tissue oximeter, this instrument can also be applied to the field of sports medicine. The usefulness of this instrument in assessing muscle tissue activity has been demonstrated.^{14,15}

However, conventional tissue oximeters are not portable and require the subject to be immobilized during use. Lasers have been used in most conventional tissue oximeters, but De Blasi et al. used light-emitting diodes (LED) as a light source.¹⁶ We

have also demonstrated that light-emitting diodes can be used and have developed the first portable tissue oximeter, which uses a two-wavelength LED.¹⁷ This newly developed oximeter is compact enough to be portable, and it is therefore expected to make better use of the advantages of NIRS-based oximetry and to expand the scope of applications of tissue oxygen monitoring. The algorithm for determination of tissue oxygenation is very important as is as the hardware. Although many algorithms have been used in NIRS, there have only been a few published reports on their details. A comparative study of these algorithms has recently been carried out systematically, based on *in vivo* spectroscopic data using a wide range of wavelengths.¹⁸

In this paper, we briefly explain the construction of our new portable tissue oximeter, present an algorithm for this oximeter deduced through systematic *in vitro* experiments using a tissuelike phantom by varying blood volume and scattering intensity, and examine the accuracy of the algorithm in *in vitro* and *in vivo* measurements. Experimental results are also compared with theoretical results obtained from diffusion theory.

Address all correspondence to Toshikazu Shiga. E-mail: shiga@gw.ols.omron.co.jp



Fig. 1 The newly developed portable tissue oximeter (HEO-100).

2 CONSTRUCTION OF THE INSTRUMENT

2.1 BASIC SPECIFICATIONS

The new portable tissue oximeter we developed¹⁷ (HEO-100, Omron Ltd. Inc.) consists of a main unit and a probe unit as shown in Figure 1. The main unit consists of a one-chip central processing unit (CPU), an LED driver, an amplifier, a memory card interface, a liquid crystal display, and a power source. When the apparatus operates in an on-line mode, data are fed into a personal computer, which processes the data to display traces of tissue oxygenation. However, in an off-line mode, the main unit is driven by the battery power source and all data with respect to reflectance from the probe are stored in the memory card so that the motion of a patient/subject is not restricted during the measurement period. The probe unit, molded in elastic black silicone rubber, has a photodiode in the center and a two-wavelength, near-infrared LED on either side. The peak wavelengths of the LED are 760 and 840 nm, as shown in the emission spectra of Figure 2. Although there are some overlaps in the periphery of the spectra, the diode has sufficiently differing spectroscopic characteristics; the half-

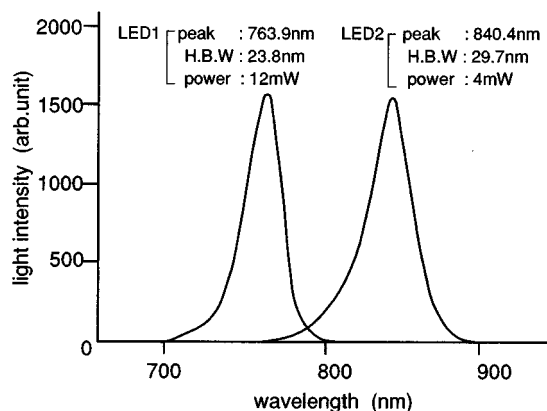


Fig. 2 Light-emission spectra of a two-wavelength near-infrared LED used in the portable tissue oximeter.

Table 1 Basic specifications of the portable tissue oximeter.

Sampling interval	0.5~120 s
Battery/Battery life	4AA batteries/6 h in case of 0.5 s sampling rate
Dimensions/Weight	85 × 42 × 160 mm (W × H × D)/340 g (excluding batteries)
Memory card/Data capacity	A 256 kbyte to 4 Mbyte SRAM card/28800 to 460800 points
Stability of measured Δ O.D.	Δ O.D. within ± 0.004 (6 h of continuous use)

widths of the spectra are 23.8 and 29.7 nm. The light-emitting intensities are 12 and 4 mW at 760 and 840 nm, respectively. These intensity levels were selected by taking into consideration the light attenuation in living tissue. Other major specifications are summarized in Table 1.

2.2 PRINCIPLE OF THE ALGORITHM

Tissue oximetry using near infrared spectroscopy is based on the modified Beer-Lambert law. The following equations are utilized as the basic equations:

$$\Delta OD_{840} = k_1 \Delta[\text{HbO}_2] + k_1' \Delta[\text{Hb}] \quad (1)$$

$$\Delta OD_{760} = k_2 \Delta[\text{HbO}_2] + k_2' \Delta[\text{Hb}], \quad (2)$$

where ΔOD_{840} and ΔOD_{760} indicate changes in optical density at 840 and 760 nm, respectively; and $\Delta[\text{HbO}_2]$ and $\Delta[\text{Hb}]$ denote changes in the concentrations of HbO_2 and Hb , respectively. The coefficients k_1 , k_1' , k_2 and k_2' are assumed to be constant, although they are dependent upon absorption and scattering when the concentrations vary greatly. The following equations are obtained from Eqs. (1) and (2).

$$\Delta[\text{HbO}_2] = K[\Delta OD_{840} - (k_1'/k_2')\Delta OD_{760}] \quad (3)$$

$$\Delta[\text{Hb}] = K(k_2/k_2')((k_1/k_2)\Delta OD_{760} - \Delta OD_{840}), \quad (4)$$

where K is equal to $k_2'/(k_1k_2' - k_1'k_2) = (1/k_2)/(k_1/k_2 - k_1'/k_2')$.

ΔBV , which indicates change in blood volume, i.e., change in the total amount of hemoglobin, is obtained as the sum of $\Delta[\text{HbO}_2]$ and $\Delta[\text{Hb}]$:

$$\begin{aligned} \Delta BV &= \Delta[\text{HbO}_2] + \Delta[\text{Hb}] \\ &= K[(1 - k_2/k_2')\Delta OD_{840} + ((k_2/k_2')(k_1/k_2) \\ &\quad - (k_1'/k_2'))\Delta OD_{760}]. \end{aligned} \quad (5)$$

The ratios k_1/k_2 , k_1'/k_2' and k_2/k_2' can be experimentally determined by measuring the ratios of

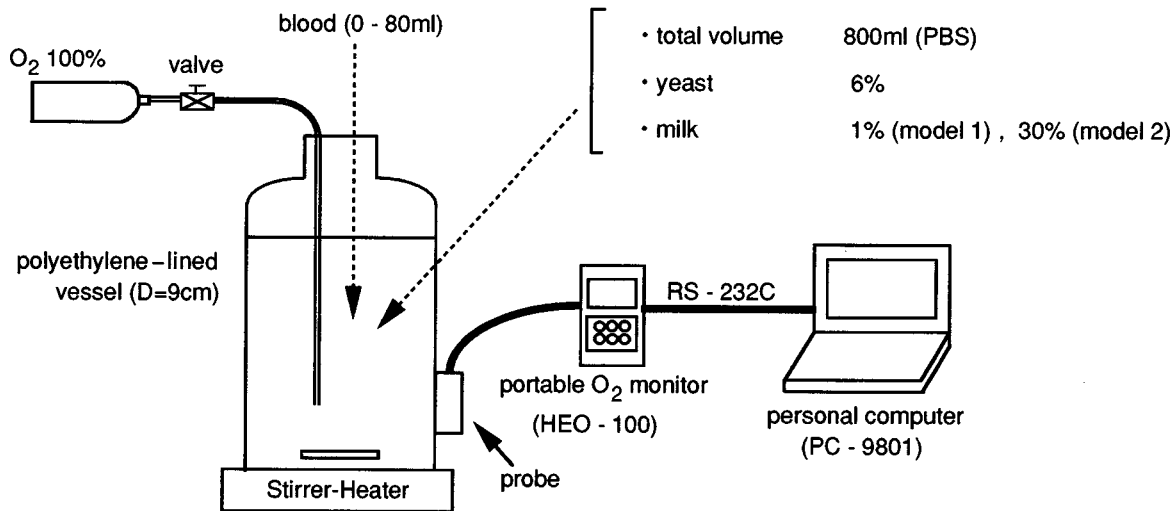


Fig. 3 Outline of the model experimental setup.

optical density changes in a fully oxygenated state (oxy) and a fully deoxygenated state (deoxy),^{19,20}

$$k1'/k2' = \Delta OD_{840} / \Delta OD_{760} \text{ in deoxy} \quad (6)$$

$$k1/k2 = \Delta OD_{840} / \Delta OD_{760} \text{ in oxy} \quad (7)$$

$$k2/k2' = \Delta OD_{760} \text{ in oxy} / \Delta OD_{760} \text{ in deoxy.} \quad (8)$$

These coefficients were determined from *in vitro* experiments, as described in the next section. K is tentatively considered to be 1, although this coefficient can be determined if a differential path length²¹ involved in $k2$ is available.

3 MODEL EXPERIMENT

3.1 METHODS

The experimental setup is shown in Figure 3. A 40- μm -thick polyethylene bag placed within a cylindrical polyethylene vessel, 9 cm in diameter, was filled with phosphate-buffered saline (PBS). The probe of the oximeter was attached to the polyethylene bag through a window made on the wall of the vessel. A nondrying immersion oil for microscopy (R.P. Cargille Laboratories, Inc.) was used for optically good contact between the probe and the bag. The source to detector distance was 20 mm. To simulate oxygen consumption in living tissue, yeast was added to the PBS at a concentration of 6% in volume. Milk, serving as a scatterer, was then added to the yeast-PBS mixture, so that the final total volume of the mixture became 800 ml. The concentration of milk in the mixture was set at either 1% (model 1) or 30% (model 2). The liquid in the container was gently stirred with a magnetic stirrer. The temperature of the liquid was maintained at 35 to 37°C. Blood was added to the vessel

in steps (4 to 5 ml/step) to vary the concentration of red blood cells between 0 and about 2.5% in volume. At each red blood cell concentration, the model was exposed to bubbling oxygen gas in order to fully oxygenate the hemoglobin. The oxygen gas supply was then shut off to allow the oxygen in the model to be consumed by the yeast and to induce deoxygenation of the hemoglobin. Almost complete oxygenation and deoxygenation of the hemoglobin was confirmed by checking that the light intensity had reached a plateau. Data sampled every 1.0 s were fed into a personal computer in the on-line mode and saved as a file. The optical density changes from an initial state (0% blood cells) after oxygenation or deoxygenation were obtained at each blood cell concentration. The same experiment was performed on both models 1 and 2.

In order to determine the optical properties of the models, measurements were repeated using black India ink instead of red blood cells as an absorber, the extinction coefficient of which was measured by a spectrophotometer (U-3410, Hitachi). In this experiment, we used a probe that has a 30 mm source-to-detector distance owing to the smaller attenuation in this model. Reduced scattering coefficients of the model were then determined by curve fitting between the experimental data and the theoretical curves of changes in optical density that were obtained from diffusion theory. For the determination of absorption and scattering, a spatially resolved technique based on diffusion theory has been proposed²² and applied to *in vivo* and *in vitro* measurement.^{23,24} In this theory, attenuation is described as a function of the effective attenuation coefficient μ_{eff} . The change in optical density is approximately given by the following equation.²⁴

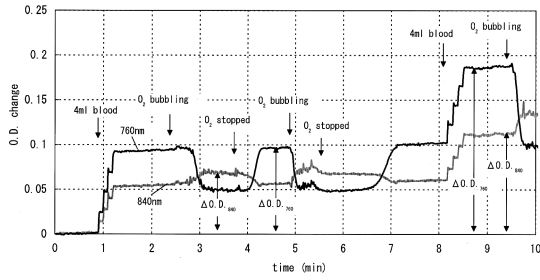


Fig. 4 An example of traces obtained by the model experiment in the case of model 1. The changes in OD from the initial state were read from the traces in fully oxygenated and deoxygenated states.

$$\Delta OD = \frac{1}{2.303} \left\{ \ln \frac{1 + \rho \mu_{\text{eff}}}{1 + \rho \mu_{\text{eff}}(0)} - \rho (\mu_{\text{eff}} - \mu_{\text{eff}}(0)) \right\}, \quad (9)$$

where ρ is the source-detector distance, $\mu_{\text{eff}} = [3\mu_a(\mu_a + \mu_s)]^{1/2}$, and $\mu_{\text{eff}}(0)$ is μ_{eff} in a reference state.

3.2 EXPERIMENTAL RESULTS

Figure 4 shows an example of traces obtained by the model experiments. The changes in OD from the initial state were read from the traces in fully oxygenated and deoxygenated states and plotted against the red blood cell concentration, as shown in Figure 5. Figures 5(a) and 5(b) show the results obtained for models 1 and 2, respectively. Solid lines indicate theoretical results obtained from Eq. (9). In the calculation, we used an absorption coefficient of hemoglobin converted from the volume percent of red blood cells and a reduced scattering

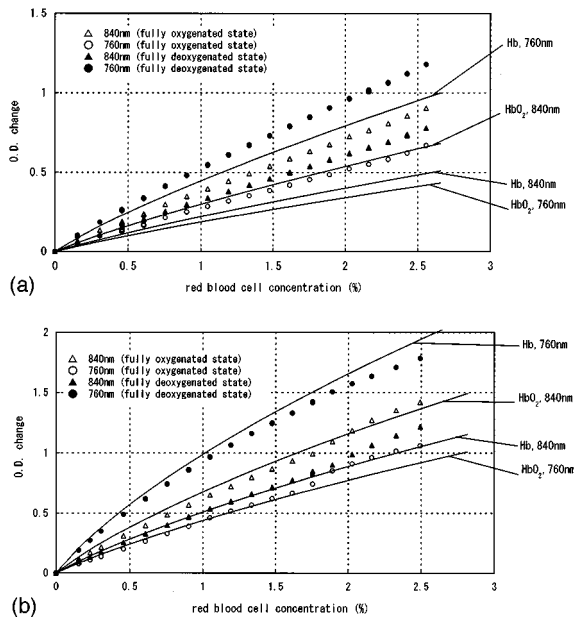


Fig. 5 Relationships between changes in OD and red blood cell concentration in (a) model 1 and (b) model 2. Solid lines indicate theoretical results obtained by the diffusion theory shown in Eq. (9).

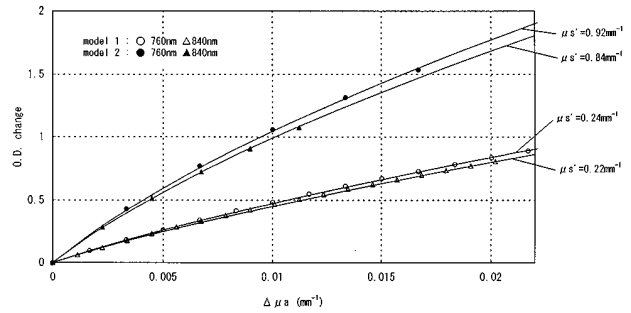


Fig. 6 Changes in OD in response to changes in the concentration of black India ink. Solid lines indicate theoretical curves drawn by reduced scattering coefficients that provided the best fit to the plots.

coefficient that was determined by results of the experiment using ink, which is shown in Figure 6. Both the experimental and theoretical results show a nonlinear relationship of change in OD in response to change in the red blood cell concentration. Nonlinearity was more marked in model 2 than in model 1. The ΔOD of deoxygenated hemoglobin at 760 nm, with a relatively high extinction coefficient, showed the strongest nonlinearity.

Figure 6 shows changes in OD in the model in which black India ink was used as an absorber. The theoretical curves were drawn by obtaining the reduced scattering coefficients that provided the best fitting to the plots. In the calculation, the absorption coefficient of water (0.003 mm^{-1}) was taken into account. Absorption due to the milk and yeast was ignored because it was negligible. The reduced scattering coefficients (base e) of the models were estimated to be 0.24 mm^{-1} at 760 nm and 0.22 mm^{-1} at 840 nm in model 1, and 0.92 mm^{-1} at 760 nm and 0.84 mm^{-1} at 840 nm in model 2.

The nonlinear relationship between absorption and optical density change in highly scattering media is known as a multiple scattering effect.²⁵ As shown in Figure 5, the experimental data obtained from model 1 are larger than the theoretical curves. On the other hand, in model 2, the theoretical curves are nearly consistent with the experimental data in model 2. Although more detailed experiments are needed to clarify the discrepancy in the curves in model 1, it seems to be due to increased scattering caused by red blood cells. In model 1, which has lower-scattering media, the influence of scattering by red blood cells is considered to be relatively large and cannot be ignored.

4 DETERMINATION OF THE ALGORITHM

Because of the nonlinear relationship between changes in OD and the red blood cell concentration, the coefficients $k1/k2$, $k1'/k2'$ and $k2/k2'$ were determined from the slopes of the experimental curves at different red blood cell concentrations. In the calculation of the slope, nonlinear regression

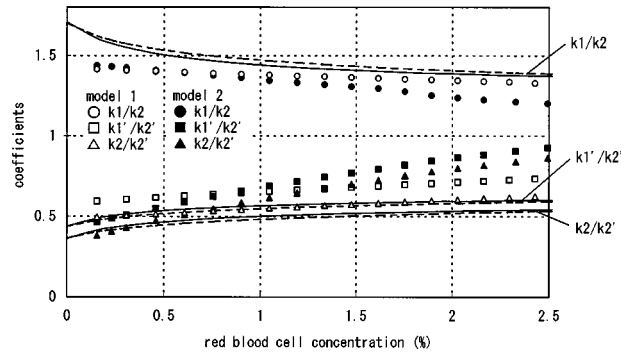


Fig. 7 Dependence of coefficients for the algorithm on red blood cell concentration. Theoretical curves are drawn by dashed lines (model 1) and solid lines (model 2). k_1/k_2 : open circles, model 1; closed circles, model 2; k_1'/k_2' : open squares, model 1; closed squares, model 2; k_2/k_2' : open triangles, model 1; closed triangles, model 2.

was applied to the plotted data in order to eliminate errors due to obtaining the slope directly from the plots. The ratios of the slopes equivalent to the coefficients defined by Eqs. (6) through (8) were then calculated under various concentrations of red blood cells; e.g., k_1/k_2 can be determined from the slopes of the curves obtained at a fully oxygenated state. As shown in Figure 7, the calculated coefficients depended on the concentration of red blood cells, the coefficients obtained from model 2 are more dependent on the red blood cell concentration than those obtained from model 1. Therefore, we averaged the values for a red blood cell concentration range of 0 to 2%, because the upper limit of the range was roughly two times as much as the tissue hematocrit of the resting skeletal muscle, which is considered to be about 1%.¹⁴ The averaged coefficients k_1/k_2 , k_1'/k_2' and k_2/k_2' were 1.39, 0.65, and 0.547 in model 1; and 1.35, 0.661, and 0.587 in model 2. The solid lines drawn in Figure 7 indicate the theoretically obtained coefficients, which show a tendency similar to the experimental results. A detailed comparison between them is given in Sec. 6. We adopted the coefficients in model 2 because the reduced scattering coefficient value was close to that of biological tissues. Thus, we obtained the following equations for operation:

$$\Delta[\text{HbO}_2] = \Delta \text{OD}_{840} - 0.66 \Delta \text{OD}_{760} \quad (10)$$

$$\Delta[\text{Hb}] = 0.80 \Delta \text{OD}_{760} - 0.59 \Delta \text{OD}_{840} \quad (11)$$

$$\Delta \text{BV} = 0.41 \Delta \text{OD}_{840} + 0.14 \Delta \text{OD}_{760} \quad (12)$$

5 VALIDATION OF THE ALGORITHM

5.1 ERRORS IN CALCULATION

Errors in calculation using the above-mentioned algorithm were analyzed. Concentration changes, $\Delta[\text{HbO}_2]$, $\Delta[\text{Hb}]$, and ΔBV , recalculated from the

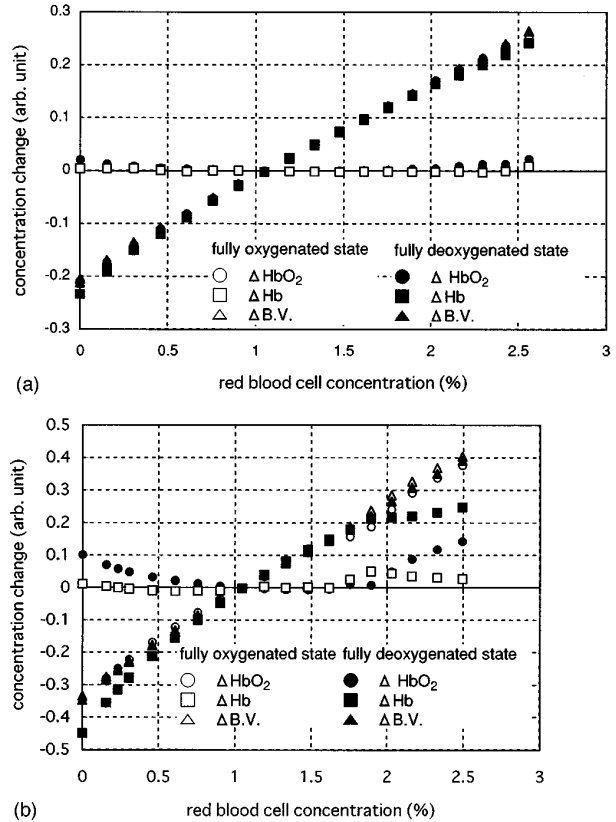


Fig. 8 Recalculation of $\Delta[\text{HbO}_2]$, $\Delta[\text{Hb}]$, and ΔBV using the determined algorithm (a, model 1; b, model 2). Normalization was done at a red blood cell concentration of 1%. Open circles, squares and triangles indicate $\Delta[\text{HbO}_2]$, $\Delta[\text{Hb}]$, and ΔBV , respectively, calculated by applying the algorithm to data obtained in a fully oxygenated state during the model experiment. Closed circles, squares and triangles indicate the same parameters calculated by applying the algorithm to data obtained in a fully deoxygenated state.

data of the model experiment using this algorithm, were compared with the varying known concentrations of red blood cells. The results are shown in Figure 8. In this figure, changes from a reference concentration of 1% are plotted, since a red blood cell concentration of 0% is not practical, and the coefficients of the equations were determined at about 1% of the concentration by the averaging. As for blood volume (indicated by triangles), there was no significant difference between oxygenated and deoxygenated states in both models. This means that calculation of blood volume using the present algorithm is little affected by the state of oxygenation. That is, the cross-talk between blood volume and two other parameters of oxygenation was almost negligible over the entire range of 0 to 2.5%.

As for $\Delta[\text{HbO}_2]$ and $\Delta[\text{Hb}]$, the discrepancy between oxygenated and deoxygenated states was also small (less than 10%) in the case of model 1, but the discrepancy in model 2 was significantly large (up to 25%). Particularly in a fully deoxygenated state, there was marked cross-talk between

$\Delta[\text{HbO}_2]$ and $\Delta[\text{Hb}]$ because of the strong nonlinear relationship between changes in OD and red blood cell concentration, as shown in Figure 5(b).

5.2 IN VIVO MEASUREMENTS

Figure 9 shows an example of tissue oximetry using the above-mentioned algorithm upon human brachia; the source–detector distance was 30 mm. Blood volume increases with venous occlusion. Oxygen saturation in mixed venous blood of healthy subjects is reported to be about 70 to 80%. Assuming that oxygen saturation of venous blood in the brachium at rest is also identical, it is likely that an increase in blood volume by venous occlusion will be accompanied by an increase in HbO_2 and Hb concentrations. During the period of complete arterial and venous occlusion, there was no significant change in blood volume, while HbO_2 decreased and Hb increased due to oxygen consumption of tissue at the same rate of concentration change.

6 DISCUSSION

As estimated from diffusion theory and shown in Figures 5 and 6, there was a nonlinear relationship between change in optical density and absorption, which is known as a multiple scattering effect in turbid media.²⁵ Therefore, the linear relation of optical density change to absorption is not exactly applicable to the algorithm for tissue oximetry. For simplicity, most of the algorithms are based on a linear relationship in which only a linear approximation of a small deviation from an appropriate operating point is valid. Hence, the effects of nonlinearity on the proportional constants of the algorithm are important. These effects are discussed in the following paragraphs.

When pure absorption without scattering is assumed, the proportional constants of an algorithm can be determined from the molecular extinction coefficients; the constants are given by the ratios of the extinction coefficients. However, this relationship is not strictly applicable to absorption in scattering media. To obtain the theoretical constants, including the effects of nonlinearity, we differentiated Eq. (9) with respect to the absorption coefficient and obtained the ratio of the derivatives. The final form of the coefficient corresponding to each equating of Eqs. (6) through (8) is given by the following equations. Details of derivation of the equation and other experimental results will be reported elsewhere.

$$\frac{k_a}{k_b} = \left(\frac{\epsilon_a \mu'_s a}{\epsilon_b \mu'_s b} \right) \left(\frac{1 + \mu_{\text{eff}} b \rho}{1 + \mu_{\text{eff}} a \rho} \right), \quad (13)$$

where ϵ is a molecular extinction coefficient. The theoretical curves in Figure 7 were drawn from this

equation. It should be stressed that, when assuming $\mu_{\text{eff}} \rho \gg 1$, the coefficient is given by the square root of that of $\mu_{\text{eff}} \rho \ll 1$.

$$\frac{k_a}{k_b} = \sqrt{\frac{\epsilon_a \mu'_s a}{\epsilon_b \mu'_s b}} \quad \mu_{\text{eff}} \rho \gg 1 \quad (14)$$

$$\frac{k_a}{k_b} = \frac{\epsilon_a \mu'_s a}{\epsilon_b \mu'_s b} \quad \mu_{\text{eff}} \rho \ll 1. \quad (15)$$

In both the experimental and the theoretical results, the proportional coefficients gradually increased ($k_1'/k_2', k_2/k_2'$) or decreased (k_1/k_2) with the red blood cell concentration. The tendencies in both results are in close agreement. However, whereas the theoretical curves reached plateaus corresponding to Eq. (14), the experimental results, particularly for model 2, were greatly affected by the red blood cell concentration. The reason for this is unknown. It might be due to error in the calculation of the gradients using nonlinear regression, because the ratio of gradients is sensitive to errors. In comparison with these coefficients, the coefficients estimated directly from the extinction coefficients, assuming scatteringless media, were significantly higher ($k_1/k_2 = 1.82$) or lower ($k_1'/k_2' = 0.467$, $k_2/k_2' = 0.364$) and were thus considered to be inappropriate for *in vivo* measurement, because $\mu_{\text{eff}} \rho \gg 1$ in most living tissues.

A linear relationship between the red blood cell concentration and change in OD was demonstrated in *in vivo* measurement of rat skeletal muscles by Seiyama, Hazeki, and Tamura.²⁰ They measured changes in OD at 700, 730, and 805 nm, perfusing oxygenated and deoxygenated blood into the muscle by varying the hematocrit from 15 to 50%. Although we cannot directly compare the linearity of our data with their results because of the differences in the wavelengths and source–detector distances used, the linearity shown in their study seems to be attributable to a relatively small change in the concentration of blood. They also determined the ratio of absorption coefficients of blood for the algorithm at two wavelengths and found the difference in the ratios between *in vivo* measurements on the rat skeletal muscle and *in vitro* measurements by hemoglobin solutions. It should be noted that the ratios shown in Table 1 of their paper also approximately satisfy the relation of the square root of extinction coefficients described above.

The dependence of proportional coefficients on the red blood cell concentration produces errors in the tissue oxygenation measured. When data from the model experiment were subjected to recalculation for the evaluation of our algorithm shown in Figure 8, we found that errors were most greatly affected by the relatively strong nonlinearity of the optical density change at 760 nm in a fully deoxygenated state, which causes cross-talk between HbO_2 and Hb. However, when the red blood cell

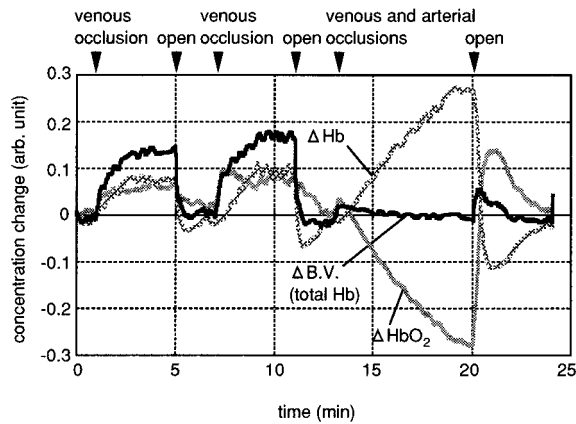


Fig. 9 An example of traces of $\Delta[\text{HbO}_2]$, $\Delta[\text{Hb}]$, and ΔBV (total Hb) calculated by applying the determined algorithm during venous and arterial occlusion of the forearm.

concentration change is within about $\pm 0.5\%$ of the initial concentration of 1%, the measured concentration is almost linear. Therefore, within a $\pm 50\%$ change from the reference concentration, the algorithm provides a relatively good linear response to the concentration. In most *in vivo* measurements, the concentration change is within this range except for severe ischemia such as an occlusion test of long duration shown in Figure 9. Measurement during exercise is also not significantly affected by the error, because the change in blood volume is smaller during exercise than during occlusion. However, care is needed in some cases, e.g., when the blood volume might decrease markedly due to muscle milking during isometric exercise.

In our algorithm, the value of K was tentatively 1. Since $K = (1/k_2) / (k_1/k_2 - k_1'/k_2')$, only k_2 is unknown. This value can be determined by the molecular extinction coefficient for HbO_2 at 760 nm, which is multiplied by a differential path length.²¹ Assuming a differential path length factor of 4.5 for the forearm,²⁶ we obtain $k_2 = 8.2$ (OD mM^{-1}) and then $K = 0.18$ (mM OD^{-1}). If $\Delta[\text{HbO}_2]$ and $\Delta[\text{Hb}]$ measured by our apparatus are multiplied by K , the absolute concentration changes can be determined. Although Figure 9 shows only one set of traces as an example of our series of measurements (T. Shiga and K. Tanabe, unpublished data), a falling rate of HbO_2 estimated from the trace becomes 0.0087 mM/min . Considering individual differences among subjects, this value is almost consistent with published data.¹⁸

7 CONCLUSIONS

We deduced an algorithm for the portable tissue oximeter using a tissuelike phantom in which the concentration of oxygenated and deoxygenated blood and the scattering intensity were varied. The experimental results were compared with the theoretical results obtained by diffusion theory. The

proportional coefficients for the algorithm, which were experimentally determined and theoretically estimated, were found to be affected by blood concentration, because of nonlinearity due to the multiple scattering effect. The results confirmed that a good linear response to the concentration of oxygenated and deoxygenated blood is obtained by this algorithm within a range of about a $\pm 50\%$ change in concentration from an initial state.

Acknowledgment

This research was supported in part by the grant-in-aid for scientific research from the Ministry of Education, Science and Culture in Japan.

REFERENCES

1. M. Tamura and T. Tamura, "Non-invasive monitoring of brain oxygen sufficiency on cardiopulmonary bypass patients by near-infrared laser spectrophotometry," *Med. Biol. Eng. Comput.* **32**, S151-S156 (1994).
2. M. Ferrari, E. Zanette, I. Giannini, G. Sideri, C. Fieschi, and A. Carpi, "Effect of carotid artery compression test on regional cerebral blood volume, hemoglobin oxygen saturation and cytochrome-c-oxidase redox level in cerebrovascular patients," *Adv. Exp. Med. Biol.* **200**, 213-222 (1986).
3. C. D. Kurth, J. M. Steven, S. C. Nicolson, and B. Chance, "Cerebral oxygenation during pediatric cardiac surgery using deep hypothermic circulatory arrest," *Anesthesiology* **82**, 74-82 (1995).
4. J. E. Brazy, D. V. Lewis, M. H. Mitnick, and F. F. Jobsis, "Noninvasive monitoring of cerebral oxygenation in pre-term infants: preliminary observations," *Pediatrics*, **75**, 217-225 (1985).
5. J. S. Wyatt, M. Cope, D. T. Delpy, S. Wray, and E. O. R. Reynolds, "Quantification of cerebral oxygenation and hemodynamics in sick newborn infants by near infrared spectrophotometry," *Lancet* **2**, 1063-1066 (1986).
6. P. Rolfe, M. Thorniley, and Y. A. B. D. Wickramasinghe, "The potential of near infrared spectroscopy for detection of fetal cerebral hypoxia," *Eur. J. Gynecol. Obstet.* **42**, 24-28 (1991).
7. M. Cope and D. T. Delpy, "System for long term measurement of cerebral blood and tissue oxygenation on infants by near infrared transillumination," *Med. Biol. Eng. Comput.* **26**, 289-294 (1988).
8. S. Gopinath, C. Robertson, R. Grossman, and B. Chance, "Near-infrared spectroscopic localization of intracranial hematomas," *J. Neurosurg.* **79**, 43-47 (1993).
9. K. K. McCully, C. Halber, and D. J. Posner, "Exercise-induced changes in oxygen saturation in the calf muscles of elderly subjects with peripheral vascular disease," *J. Gerontol.:Biol. Sci.* **49**(3), 128-134 (1994).
10. J. R. Wilson, D. M. Mancini, K. McCully, N. Ferraro, V. Lanocce, and B. Chance, "Noninvasive detection of skeletal muscle underperfusion with near-infrared spectroscopy in patients with heart failure," *Circulation* **80**, 1668-1674 (1989).
11. T. Komiyama, H. Shigematsu, H. Yasuhara, and T. Muto, "An objective assessment of intermittent claudication by near-infrared spectroscopy," *Eur. J. Vasc. Surg.* **8**, 294-296 (1994).
12. T. Ozawa, K. Sahashi, Y. Nakase, and B. Chance, "Extensive tissue oxygenation associated with mitochondrial DNA mutations," *Biomed. Biophys. Res. Comm.* **213**(2), 432-438 (1995).
13. T. Hamaoka, K. McCully, B. Chance, and H. Iwane, "Non-invasive measures of muscle metabolism," in *Exercise and Oxygen Toxicity*, C. K. Sen, P. Lester, and H. Osmo, Eds., pp. 481-510, Elsevier, Amsterdam (1994).
14. B. Chance, M. T. Dait, C. Zhang, T. Hamaoka, and F. Hagerman, "Recovery from exercise-induced desaturation in the quadriceps muscles of elite competitive rowers," *Am. J. Physiol.* **262**, 766-775 (1992).

15. T. Hamaoka, C. Albani, B. Chance, and H. Iwane, "A new method for the evaluation of muscle aerobic capacity in relation to physical activity measured by near-infrared spectroscopy," *Med. Sport. Sci.* **37**, 421–429 (1992).
16. R. A. De Blasi, S. Fantini, M. A. Franceschini, M. Ferrari, and E. Gratton, "Cerebral and muscle oxygen saturation measurement by frequency-domain near-infrared spectrometer," *Med. Biol. Eng. Comput.* **33**, 228–230 (1995).
17. T. Shiga, K. Tanabe, Y. Nakase, T. Shida, and B. Chance, "Development of a portable tissue oximeter using near infrared spectroscopy," *Med. Biol. Eng. Comput.* **33**, 622–626 (1995).
18. S. J. Matcher, C. E. Elwell, C. E. Cooper, M. Cope, and D. T. Delpy, "Performance comparison of several published tissue near-infrared spectroscopy algorithms," *Anal. Biochem.* **227**, 54–68 (1995).
19. O. Hazeki and M. Tamura, "Quantitative analysis of hemoglobin oxygenation state of rat brain *in situ* by near-infrared spectrophotometry," *J. Appl. Physiol.* **64**(2), 796–802 (1988).
20. A. Seiyama, O. Hazeki, and M. Tamura, "Noninvasive quantitative analysis of blood oxygenation in rat skeletal muscle," *J. Biochem.* **103**, 419–424 (1988).
21. D. T. Delpy, M. Cope, P. vander Zee, S. Arridge, S. Wray, and J. Wyatt, "Estimation of optical pathlength through tissue from direct time of flight measurement," *Phys. Med. Biol.* **33**, 1433–1442 (1988).
22. T. J. Farrell, M. S. Patterson, and B. Wilson, "A diffusion theory model of spatially resolved, steady-state diffuse reflectance for the noninvasive determination of tissue optical properties *in vivo*," *Med. Phys.* **19**, 879–888 (1992).
23. S. J. Matcher, P. Kirkpatrick, K. Nahid, M. Cope, and D. T. Delpy, "Absolute quantification methods in tissue near infrared spectroscopy," *Proc. SPIE* **2389**, 486–495 (1995).
24. H. Liu, D. A. Boas, Y. Zhang, A. G. Yodh, and B. Chance, "Determination of optical properties and blood oxygenation in tissue using continuous NIR light," *Phys. Med. Biol.* **40**, 1983–1993 (1995).
25. M. Cope, P. van der Zee, M. Essenpreis, S. R. Arridge, and D. T. Delpy, "Data analysis methods for near infrared spectroscopy of tissue: problems in determining the relative cytochrome *aa3* concentration," *Proc. SPIE* **1431**, 251–262 (1991).
26. M. Essenpreis, C. E. Elwell, M. Cope, P. van der Zee, S. R. Arridge, and D. T. Delpy, "Spectral dependence of temporal point spread functions in human tissues," *Appl. Opt.* **32**, 418–425 (1993).